2-17-2017

Mass-Analyzed Threshold Ionization Spectroscopy of Lanthanum-Hydrocarbon Radicals Formed by C—H Bond Activation of Propene

Sudesh Kumari
University of Kentucky, sudeshchem@gmail.com

Wenjin Cao
University of Kentucky, wj.cao0707@uky.edu

Dilrukshi C. Hewage
University of Kentucky, hewagedilrukshi@gmail.com

Ruchira Silva
University of Kentucky

Dong-Sheng Yang
University of Kentucky, dyang0@uky.edu

Mass-Analyzed Threshold Ionization Spectroscopy of Lanthanum-Hydrocarbon Radicals Formed by C—H Bond Activation of Propene

Digital Object Identifier (DOI)
https://doi.org/10.1063/1.4976316

Mass-analyzed threshold ionization spectroscopy of lanthanum-hydrocarbon radicals formed by C—H bond activation of propene

Sudesh Kumari, Wenjin Cao, Dilrukshi Hewage, Ruchira Silva, and Dong-Sheng Yang[a)]
Department of Chemistry, University of Kentucky, Lexington, Kentucky 40506-0055, USA

(Received 14 December 2016; accepted 31 January 2017; published online 17 February 2017)

$La(C_3H_4)$ and $La(C_3H_6)$ are observed from the reaction of laser-vaporized La atoms with propene by photoionization time-of-flight mass spectrometry and characterized by mass-analyzed threshold ionization spectroscopy. Two isomers of $La(C_3H_4)$ are identified as methyl-lanthanacyclopropene [$La(CHCCH_3)$] (C_s) and lanthanacyclobutene [$La(CHCHCH_2)$] (C_1); $La(C_3H_6)$ is determined to be H—La(η^3-allyl) (C_s), a C—H bond inserted species. All three metal-hydrocarbon radicals prefer a doublet ground state with a La 6s-based electron configuration. Ionization of the neutral doublet state of each of these radicals produces a singlet ion state by removing the La-based 6s electron. The threshold ionization allows accurate measurements of the adiabatic ionization energy of the neutral doublet state and metal-ligand and ligand-based vibrational frequencies of the neutral and ionic states. The formation of the three radicals is investigated by density functional theory computations. The inserted species is formed by La inserting into an allylic C—H bond and lanthanacyclopropene by concerted vinylic H_2 elimination, whereas lanthanacyclobutene involves both allylic and vinylic dehydrogenations. The inserted species is identified as an intermediate for the formation of lanthanacyclobutene. *Published by AIP Publishing.* [http://dx.doi.org/10.1063/1.4976316]

I. INTRODUCTION

C—H bonds are ubiquitous in organic molecules, yet many of these are chemically inert under mild conditions because of their highly thermodynamic stability. Metal activation circumvents this problem by stimulating the inert C—H bonds to react with other molecules. The goal of designing selective and effective metal agents for such reactions has stimulated extensive research activities in solution[1–7] and gas[8–15] phases. Gas-phase studies of metal-mediated hydrocarbon activation provide an efficient means to investigate intrinsic reactivity patterns, reaction paths, and structure-reactivity relationships without interferences from solvents and counterions. Such studies are also pertinent to the recent studies on single-metal-atom catalysts.[16–20]

Previous experimental studies in the gas phase were largely focused on the measurements of reaction kinetics and thermodynamics,[8–15] which are essential but not sufficient for devising plausible reaction mechanisms. The other critical piece of information is the geometries and electronic states of the reaction intermediates and products. Quantum chemical calculations can be used to predict the structures and electronic states for such species. However, a reliable prediction of low-energy electronic states and molecular structures of transition-metal or f-block organometallic complexes is complicated by the possibility of multiple low-energy structural isomers of each complex and many low-energy states or spin-orbit levels of each isomer. Therefore, a reliable identification of structural isomers and electronic states generally requires confirmation by spectroscopic measurements.[21–28]

As one of the simplest alkene molecules and the most important raw chemicals in petrochemical industry, metal-mediated propene activation has been extensively studied in the gas phase. Its reactions with metal ions were mainly studied with Fourier-transform ion-cyclotron resonance, guided-ion-beam, or other mass-spectrometry based methods.[8,29–36] Neutral metal atom reactions are more difficult to study because reaction products cannot be followed directly by mass spectrometry. Alternatively, reactions with the neutral atoms were monitored by photoionization mass spectrometry of resultant species or laser-induced fluorescence measurements of the depletion of the metal atom concentration.[9,37–43] To our knowledge there has been no spectroscopic measurement for the metal atom-mediated propene activation in the gas phase, partly because of the low number density of the reactive species produced in such reactions. In this paper, we report the time-of-flight (TOF) mass spectrometric observation of the metal-hydrocarbon radicals formed by the La + propene reaction, mass-analyzed threshold ionization (MATI) spectroscopic characterization of the geometric structures and electronic states of $La(C_3H_4)$ and $La(C_3H_6)$ formed by the C—H bond activation, and density functional theory (DFT) predicted pathways for the formation of the insertion and dehydrogenation species. This work continues our recent efforts on spectroscopic characterization of lanthanide-mediated hydrocarbon activation reactions.[44–47]

[a)]Author to whom correspondence should be addressed. Electronic mail: dyang0@uky.edu

II. EXPERIMENTAL AND COMPUTATIONAL METHODS

The metal-cluster beam instrument used in this work consists of reaction and spectroscopy vacuum chambers and was described in a previous publication.[48] The metal-hydrocarbon reaction was carried out in a laser vaporization metal cluster beam source. Propene (99+%, Aldrich) was seeded in a He, Ar, or He/Ar carrier gas with a concentration of 10^{-4}-10^{-6} in a stainless steel mixing cylinder. La atoms were generated by pulsed-laser (Nd:YAG, Continuum Minilite II, 532 nm, ~2.0 mJ/pulse) vaporization of a La rod (99.9%, Alfa Aesar) in the presence of the propene/carrier gas mixture (40 psi) delivered by a home-made piezoelectric pulsed valve. The metal atoms and gas mixture entered into a collision tube (2 mm diameter and 2 cm length) and were then expanded into the reaction chamber, collimated by a cone-shaped skimmer (2 mm inner diameter), and passed through a pair of deflection plates. Ionic species in the molecular beam that were formed during laser vaporization were removed by an electric field (100 V cm^{-1}) applied on the deflection plates. The neutral products were identified by photoionization TOF mass spectrometry. A separate experiment was carried out to confirm that propene was activated by La rather than the vaporization laser. In this experiment, propene was introduced by a second pulsed valve (Parker, Series 9) 3 cm downstream of the laser vaporization point. The reaction products formed in the two experiments were identical, though a higher propene concentration in the second experiment was required to produce comparable ion intensity in the mass spectra. Because propene bypassed the vaporization region in the second experiment, direct excitation of propene via the vaporization laser played no role in the hydrocarbon activation. This was further confirmed by the 118 nm (10.508 eV) laser ionization of the molecular beam formed by passing the hydrocarbon/carrier mixture through the laser vaporization point, where no hydrocarbon species other than C_3H_6 was observed. The 118 nm laser was generated by the frequency tripling of the third harmonic output of a Nd:YAG laser (355 nm, 20 mJ/pulse) in a Xe gas cell (Xe:Ar = ~1:10 at 2 psi).

Prior to the MATI measurements, photoionization efficiency spectra of the La-hydrocarbon complexes were recorded to locate their approximate ionization thresholds to guide the survey MATI scans. In the MATI experiment, each of the La complexes was excited to high-lying Rydberg states in a single-photon process and ionized by a delayed pulsed electric field. The excitation laser was the same as that used for photoionization in the mass spectrometric and photoionization efficiency experiments and was the frequency doubled output of a tunable dye laser (Lumonics HD-500), pumped by the third harmonic output (355 nm) of a Nd:YAG laser (Continuum Surelite II). The laser beam was collinear and counter propagating with the molecular beam. The ionization pulsed field (320 V cm^{-1}) was generated by two high voltage pulse generators (DEI, PVX-4140) and delayed by 10-20 μs from the laser pulse by a delayed pulsed generator (SRS, DG645). A small DC field (6.0 V cm^{-1}) was applied to separate the ions produced by direct photoionization from the MATI ions generated by delayed field ionization. The MATI ion signal was obtained by scanning the wavelength of the tunable dye laser, detected by a dual microchannel plate detector, amplified by a preamplifier (SRS, SR445), visualized by a digital oscilloscope (Tektronix TDS 3012), and stored in a laboratory computer. Laser wavelengths were calibrated against vanadium atomic transitions in the MATI spectral region.[49] The Stark shift on the ionization energy (IE) induced by the DC separation field (E_f) was calculated using the relation of $\Delta IE = 6.1E_f^{1/2}$, where E_f is in V cm^{-1} and ΔIE is in cm^{-1}.[50]

Geometry optimization and vibrational frequency calculations were carried out using Gaussian 09 software package.[51] In these calculations, we used the Becke's three-parameter hybrid functional with the correlation functional of Lee, Yang, and Parr (B3LYP) and 6-311+G(d,p) basis set for C and H and the Stuttgart/Dresden (SDD) effective core potential basis set with 28 electron core for an La atom. We have extensively used DFT/B3LYP and found that this method generally produced adequate results for the spectral and structural assignments of organometallic radicals.[44–47,52] No symmetry restrictions were imposed on initial geometry optimizations, but appropriate point groups were used in subsequent optimizations to identify electronic symmetries. For each optimized stationary point, a vibrational analysis was performed to identify the nature of the stationary point (minimum or saddle point). In predicting reaction pathways, minima connected by a transition state were confirmed by intrinsic reaction coordinate calculations.

To compare with the experimental MATI spectra, multidimensional Franck-Condon (FC) factors were calculated from the equilibrium geometries, harmonic vibrational frequencies, and normal coordinates of the neutral and ionized complexes.[53] In these calculations, the recursion relations from the work of Doktorov *et al.*[54] were employed, and the Duschinsky effect[55] was considered to account for a possible axis rotation from the neutral complex to the cation. Spectral simulations were obtained using the experimental linewidth and Lorentzian line shape. Transitions from excited vibrational levels of the neutral complex were considered by assuming thermal excitation at specific temperatures.

III. RESULTS AND DISCUSSION

A. TOF mass spectrum and La-hydrocarbon species

Figure 1 shows the TOF mass spectrum of the La + propene reaction recorded with 220 nm (45 455 cm^{-1} or 5.636 eV) laser ionization. La is ionized by a single-photon ionization process as its IE (5.5769 eV) is lower than the laser energy used for recording the mass spectrum.[56] The IE of LaO has been reported as 4.95 (19) eV via a thermochemical analysis[57] or ≥5.19 eV by theoretical predictions.[58] Thus, LaO could be ionized via a single-photon ionization process as well. LaO could be formed by the reaction of La atoms with oxygen present in the carrier gas as an impurity or by the laser vaporization of La oxide impurity in the La rod. All La-hydrocarbon complexes are ionized through single-photon processes because the IEs of organometallic radicals are usually lower than that of the bare atoms.[44–47,52] Because the photon energy is only slightly higher than their IEs, dissociative ionization is minimized for these La-hydrocarbon

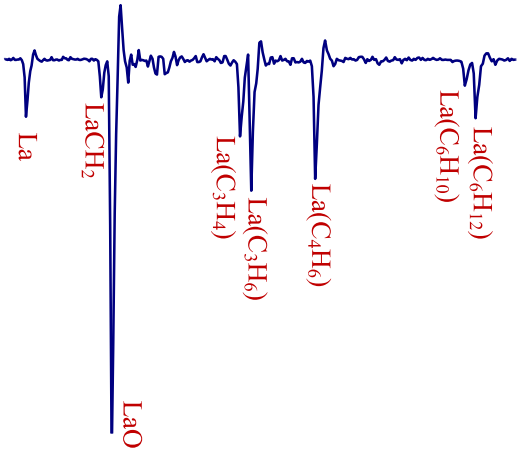

FIG. 1. TOF mass spectrum of the La + propene reaction recorded with 220 nm laser ionization.

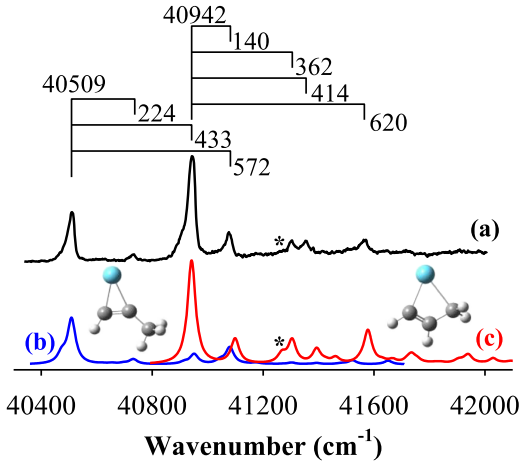

FIG. 2. MATI spectrum of $La(C_3H_4)$ seeded in 1:1 He/Ar (a) and simulations of La(CHCCH3) (C_s, $1A' \leftarrow 2A'$, 100 K, blue trace) (b) and $La(CHCHCH_2)$ (C_1, $^1A \leftarrow {}^2A$, 100 K, red trace) (c).

complexes. Therefore, the mass spectrum can be used to monitor the neutral metal complexes formed in the reaction. The resultant metal hydrocarbon complexes include $La(CH_2)$, $La(C_3H_n)$(n = 4 and 6), $La(C_4H_6)$, and $La(C_6H_m)$ (m = 10 and 12). Possibly overall reactions for the formation of these metal-hydrocarbon species are presented in Scheme 1. The primary reactions ((1a)-(1c)) include association or insertion, dehydrogenation, and C—C bond cleavage; the secondary reactions ((2a)-(2c)) involve the addition of the La-hydrocarbon species produced by the primary reactions to a second propene molecule, followed by dehydrogenation. $La(C_6H_{10})$ could also be formed by $La(C_3H_6) + C_3H_6 \rightarrow La(C_6H_{10}) + H_2$. Because it costs energies to break two C—H bonds, however, this reaction should have a smaller probability than reaction (2b). There have been no previous studies on the La + propene reaction in the gas phase, but Y (which is in the same group as La in the periodical table) reactions with propene have been reported to produce $Y(CH_2)$, $Y(C_3H_4)$, and $Y(H_2)$ in a crossed molecular beam[42] and $Y(C_3H_n)$ (n = 2, 4, and 6) in a fast flow reactor.[41] Reactions of Ce^+/La^+ with propene have also been reported, in which $M^+(CH_2)$, $M^+(C_3H_4)$, $M^+(C_4H_6)$, $M^+(C_6H_n)$ (n = 6 and 8), and $M^+(C_5H_6)$ (M^+ = Ce^+ and La^+) were observed by Fourier-transform ion cyclotron resonance mass spectrometry.[29] In Sections III B–III D, we will discuss the MATI spectra, structures, and formations of $La(C_3H_4)$ and $La(C_3H_6)$ formed by the C—H bond activation of propene.

$$La + C_3H_6 \rightarrow La(C_3H_6) \quad 1a$$
$$La + C_3H_6 \rightarrow La(C_3H_4) + H_2 \quad 1b$$
$$La + C_3H_6 \rightarrow La(CH_2) + C_2H_4 \quad 1c$$
$$La(CH_2) + C_3H_6 \rightarrow La(C_4H_6) + H_2 \quad 2a$$
$$La(C_3H_4) + C_3H_6 \rightarrow La(C_6H_{10}) \quad 2b$$
$$La(C_3H_6) + C_3H_6 \rightarrow La(C_6H_{12}) \quad 2c$$

SCHEME 1. La + propene overall reactions.

B. MATI spectrum and two isomers of $La(C_3H_4)$

The MATI spectrum of $La(C_3H_4)$ is shown in Figure 2(a). It displays the strongest band at 40 942 (5) cm^{-1}, followed by four vibrational intervals ranging from 140 to 620 cm^{-1}. The strongest band can easily be assigned to the transition between the zero vibrational levels of the neutral and ionic states of the molecule (i.e., 0-0 band). On the lower energy side of the 0-0 band, the spectrum displays the second strongest band at 40 509 (5) cm^{-1} and a weak one at 224 cm^{-1} above the 40 509 cm^{-1} band. The 40 509 cm^{-1} band is unlikely a vibrational hot band because its intensity is unusually high compared to the 40 509 + 224 cm^{-1} band but arises from the ionization of a different isomer as discussed below.

La-mediated dehydrogenation of propene could yield four isomers depending on which two hydrogen atoms are eliminated (Figure 3). 1,1-dehydrogenation leads to (prop-1-enylidene)lanthanum [La(CCHCH$_3$)], 1,2-dehydrogenation to methyl-lanthanacyclopropane [La(CHCCH$_3$)], 1,3- or 3,3-elimination to lanthanacyclobutene [La(CHCHCH$_2$)], and 2,3-elimination to methylene-lanthanacyclopropane [La(CH$_2$CCH$_2$)]. Among these isomers, $La(CHCHCH_2)$ is predicted to be the most stable one, followed by La(CHCCH$_3$)

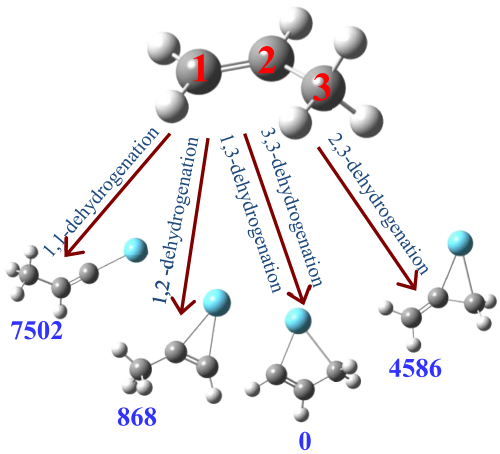

FIG. 3. Relative energies (cm^{-1}) of $La(C_3H_4)$ isomers from DFT/B3LYP calculations.

at ~0.1 eV, La(CH_2CCH_2) at ~0.6 eV, and La($CCHCH_3$) at ~0.9 eV. Because of their high energies, La(CH_2CCH_2) and La($CCHCH_3$) can be excluded from the carriers of the observed MATI spectra. Table I summarizes the DFT/B3LYP predicted electronic energies of the two lowest-energy isomers: La($CHCCH_3$) and La($CHCHCH_2$). La($CHCCH_3$) has a C_s symmetry with the three carbon atoms forming the reflection plane, whereas La($CHCHCH_2$) has no real symmetry element except for the identify. Both isomers are predicted to have a doublet ground electronic state ($^2A'$ or ^2A) with a quartet state being ~1.5 eV higher in energy. Although ionization of a double state could form singlet and triplet states, the triplet ← doublet transition can be excluded because the adiabatic IE (AIE) of this process is predicted to be much higher than the experimental value (Table I). Therefore, the best explanation for the observed spectrum is that it arises from the singlet ← doublet ionization of the La($CHCCH_3$) and La($CHCHCH_2$) isomers. By comparing the computed and measured 0-0 band energies, the $^1A' \leftarrow {}^2A'$ ionization of La($CHCCH_3$) (41 214 cm^{-1}) is assigned to the transition originating from the 40 509 cm^{-1} band and the $^1A \leftarrow {}^2A$ ionization of La($CHCHCH_2$) (41 540 cm^{-1}) to the transition associated with the 40 942 cm^{-1} band. The computed energy difference between the two 0-0 transitions is 326 cm^{-1}, comparable to the observed value of 433 cm^{-1}. La($CHCCH_3$) is predicted to be slightly higher in energy than La($CHCHCH_2$), which is consisted with the observed lower intensity of the 40 509 cm^{-1} band than that of the 40 942 cm^{-1} transition in the MATI spectrum.

The assignment of the singlet ← doublet transitions of the two isomers to the observed spectrum is further confirmed by comparing the measured spectrum with the spectral simulations in Figure 2(b). In these simulations, the calculated 0-0 transition of La($CHCCH_3$) is aligned with the 40 509 cm^{-1} band (blue trace) and that of La($CHCHCH_2$) to the 40 942 cm^{-1} band (red trace), and the vibrational frequencies of the two isomers are unscaled in order to directly compare with the experimental data. Although neither of the two simulations matches the experimental spectrum, their combination reproduces the observation quiet nicely. The vibrational assignments based on the simulations are summarized in Table II. Because of the low molecular symmetry, two La—C stretching modes are observed for La($CHCCH_3$) and three for La($CHCHCH_2$); these stretching modes are predicted to be mixed with ligand-based vibrations. For La($CHCCH_3$), the La—C2 stretch mixed with a C2—CH_3 in-plane bend (ν_{11}^+, 433 cm^{-1}) is predicted to overlap with the 0-0 transition of La($CHCHCH_2$); the La—C1 stretch mixed with a C1—H in-plane bend (ν_{10}^+, 572 cm^{-1}) overlaps with a C—C—C out-of-plane bend excitation (140 cm^{-1}) of La($CHCHCH_2$). The carbon atomic numbering is shown in Figure 4. For La($CHCHCH_2$), two of the three metal-ligand stretching modes (ν_{14}^+ and ν_{15}^+) are calculated to mix with a CH_2 rocking mode or a C—C—C in-plane bend. The CH_2 rocking mode (ν_{17}^+) (marked with "*" in Figure 2(b)) is predicted to be weakly active, which may correspond to the weak, unresolved transition around 320 cm^{-1} (marked "*" in Figure 2(a)). The higher La—C1 and C3 stretching frequency (ν_{14}^+) than the other two metal-ligand stretching modes (ν_{15}^+ and ν_{16}^+) in La($CHCHCH_2$) is consistent with their shorter La—C bond distances (Table S1 of the supplementary material). The computed AIEs are 500-700 cm^{-1} higher than the measured values, and the computational errors on the vibrational frequencies are mostly within 10-20 cm^{-1}. For both isomers, the La-valence electron configuration of the doublet ground state is $6s^1$, and ionization removes the La-based 6s electron to produce the singlet ion.

TABLE I. Point groups, electronic states, relative energies (E_{rel}, cm^{-1}), and adiabatic ionization energies (AIEs, cm^{-1}) of the La($CHCCH_3$), La($CHCHCH_2$), and H—La(η^3-C_3H_5) complexes from DFT/B3LYP calculations.

Complexes	Symmetry	States	E_{rel}	Transitions	AIE
La($CHCCH_3$)					40 509[a]
	C_s	$^3A''$	51 365	$^3A'' \leftarrow {}^2A'$	51 365
				$^3A'' \leftarrow {}^4A''$	39 993
	C_s	$^1A'$	41 214	$^1A' \leftarrow {}^2A'$	41 214
	C_s	$^4A''/^2A'$	11 371/0		
La($CHCHCH_2$)					40 942[a]
	C_1	^3A	52 435	$^3A \leftarrow {}^2A$	52 435
				$^3A \leftarrow {}^4A$	39 568
	C_1	^1A	41 540	$^1A \leftarrow {}^2A$	41 540
	C_1	$^4A/^2A$	12 867/0		
H-La(η^3-C_3H_5)					41 131
	C_s	$^3A''$	57 134	$^3A'' \leftarrow {}^2A'$	57 134
				$^3A'' \leftarrow {}^4A''$	37 303
	C_s	$^1A'$	41 669	$^1A' \leftarrow {}^2A'$	41 669
	C_s	$^4A''/^2A'$	19 831/0		

[a]From MATI spectra.

TABLE II. Adiabatic ionization energies (AIEs, cm^{-1}) and vibrational frequencies (cm^{-1}) of the La($CHCCH_3$) (C_s), La($CHCHCH_2$) (C_1), and H—La(η^3-C_3H_5) (C_s) complexes from MATI spectroscopy and DFT/B3LYP calculations. ν_n and ν_n^+ are vibrational modes in the neutral and ion states.

Complexes	MATI	B3LYP	Mode description[a]
La($CHCCH_3$) ($^1A' \leftarrow {}^2A'$)			
AIE	40 509	41 214	
v_{12}^+	224	222	C2—CH_3 in-plane bend
v_{11}^+	433	442	La—C2 stretch and C2—CH_3 in-plane bend
v_{10}^+	572	570	La—C1 stretch and C1—H in-plane bend
La($CHCHCH_2$) ($^1A \leftarrow {}^2A$)			
AIE	40 942	41 540	
v_{18}^+	140	156	C—C—C out-of-plane bend
v_{17}^+	(~320)	326	CH_2 rock
v_{16}^+	362	362	La—C2 and —C3 stretch
v_{15}^+	414	451	La—C1 and —C2 stretch and CH_2 rock
v_{14}^+	620	635	La—C1/C3 stretch and C—C—C in-plane bend
H—La(η^3-C_3H_5) ($^1A' \leftarrow {}^2A'$)			
AIE	41 131	41 669	
v_{14}^+/v_{14}	278/238	267/239	La—H and terminal C—H bond wag
v_{11}^+	475	472	Terminal CH_2 rock

[a]Carbon atomic numbering is shown in Figure 4.

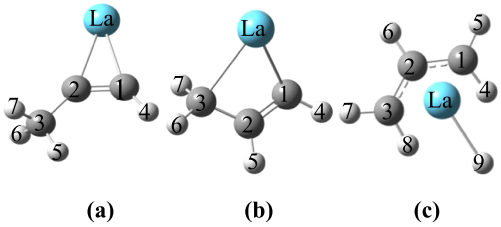

FIG. 4. Structures of La(CHCCH$_3$) (a), La(CHCHCH$_2$) (b), and H—La(η^3-C$_3$H$_5$) (c).

Because the La 6s^1 electron is not significantly involved in the bonding with the hydrocarbon fragment, its removal has a small effect on the metal-ligand distance and other geometric parameters (Table S1). This is consistent with the very short FC profiles of both species observed in the MATI spectrum.

C. MATI spectrum and inserted structure of La(C$_3$H$_6$)

The MATI spectrum of La(C$_3$H$_6$) displays a longer FC profile than those of La(CHCCH$_3$) and La(CHCHCH$_2$) as shown in Figure 5(a). It shows a progression of 278 cm^{-1} with four vibrational quanta beginning at 41 131 (5) cm^{-1}. Superimposed on the 278 cm^{-1} progression are satellite bands separated with 40 cm^{-1}. In addition, a transition is observed at 238 cm^{-1} to the red of the 41 131 cm^{-1} band. Because no additional 278 cm^{-1} intervals are observed below the 41 131 cm^{-1} band, the 41 131 cm^{-1} transition is attributed to the 0-0 transition. With the identification of the 0-0 band, the 278 cm^{-1} progression can then be assigned to the transition from the zero vibrational level of the neutral complex to various vibrational levels of the ion, the 238 cm^{-1} interval to a transition from a thermally excited vibrational level of the neutral complex, and the 40 cm^{-1} satellite bands to sequence transitions involving the 238 and 278 cm^{-1} modes of the neutral and ionic species. We tried to record MATI spectra using pure Ar to confirm the hot bands, as metal complexes seeded in heavier carriers may

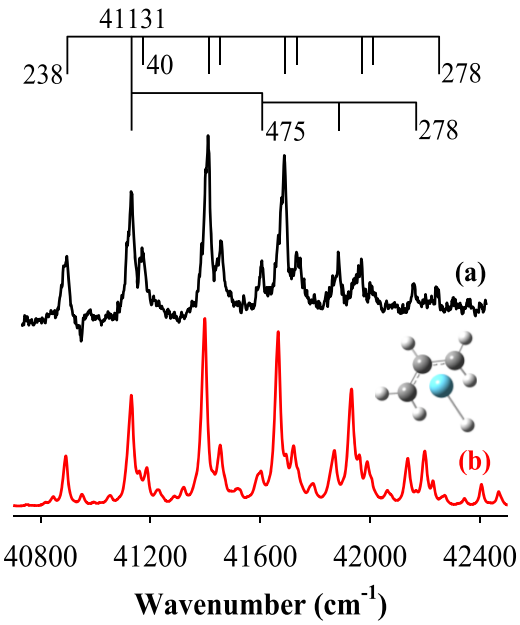

FIG. 5. MATI spectrum of La(C$_3$H$_6$) seeded in 2:1 He/Ar (a) and simulation of the 1A′ ← 2A′ transition of H—La(η^3-C$_3$H$_5$) (C$_s$) at 300 K.

have different vibrational temperatures.[59] Unfortunately, the MATI signals were too weak when pure Ar was used as the carrier gas. Nevertheless, the above assignments are supported by spectral simulations discussed below.

We have found three isomers of La(C$_3$H$_6$) using the DFT/B3LYP calculations. The most stable one is an inserted species H—La(η^3-C$_3$H$_5$) (C$_s$), followed by lanthanacyclobutane La(CH$_2$CH$_2$CH$_2$) (C$_s$) at ~0.35 eV and methyllanthanacyclopropane La(CH$_2$CHCH$_3$) (C$_1$) at ~0.56 eV in their doublet ground states (Figure 6). Like La(C$_3$H$_4$), the quartet states of all three isomers are predicted to be much higher in energy than the doublet states (Table S2). The observed isomer of La(C$_3$H$_6$) is determined to be the inserted species H—La(η^3-C$_3$H$_5$); other two isomers are not only in higher energies but also exhibit mismatched spectral profiles with the experimental spectrum (Figure S1 of the supplementary material). Although there are three possible transitions for the insertion isomer: 1A′ ← 2A′, 3A′ ← 2A′, and 3A′ ← 4A″, the spectrum shows only one band system. Thus only one transition is responsible for the observation. This transition is determined to be 1A′ ← 2A′ as its AIE (41 169 cm^{-1}) and FC profile have the best matches with the experimental observation (Table I and Figure 5). The AIEs of the other two transitions are either too high or too low (Table I). Based on the reasonable agreement between the predicted and measured spectra, the 278 cm^{-1} intervals are assigned to a La—H wag mixed with the terminal C—H wag excitations (ν_{14}^+) in the 1A′ ion state, and the 238 cm^{-1} interval is attributed to the thermal excitation of the same mode (ν_{14}) in the ^{2}A′ neutral state, the 40 cm^{-1} separation is the frequency difference between ν_{14}^+ and ν_{14}, and the 475 cm^{-1} interval is the vibrational frequency of a CH$_2$ rock mode (ν_{11}^+) in the ion state. The predicated vibrational frequencies for the ν_{14}^+, ν_{14}, and ν_{11}^+ modes are 267, 239, and 472 cm^{-1}, in excellent agreement with the measured values of 270, 238, and 475 cm^{-1}, respectively. The structure of the insertion complex in the ^{2}A′ ground state is featured with nearly identical La—C bond lengths (i.e., 2.656, 2.656, and 2.679 Å) and a short La—H distance (2.091 Å) (Table S1). The C—C bond distances are also the same, 1.404 Å, which is about the average of the C—C single (1.500 Å) and C=C double (1.331 Å) bond lengths of propene. Thus, the C$_3$H$_5$ fragment can be considered as an allyl radical. Another feature of the inserted structure is that the H—La bond is not in the CCC plane of the allyl radical, and H—La—C2 (middle point of the CCC frame) is predicted to be 121.2°. As in the case of dehydrogenated species La(C$_3$H$_4$), the La-valence configuration of the 2A′ state is 6s^1, and the removal of the La 6s^1 electron leads to the 1A′ ion state with similar geometries to the neutral doublet, except for an reduced H—La—C2 angle (i.e., from 121.2° to 109.8°) (Table S1). This structural change

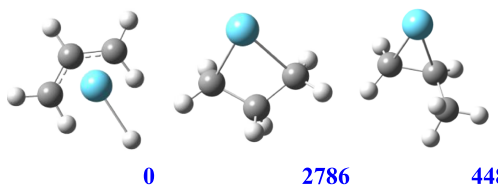

FIG. 6. Relative Energies (cm^{-1}) of La(C$_3$H$_6$) isomers from DFT/B3LYP calculations.

upon ionization is consistent with the observation of the active La—H wag mode in the MATI spectrum.

Previously, Parnis and co-workers reported a Fourier transform infrared (FTIR) matrix-isolation study of thermally vaporized vanadium atom reactions with propene in a solid Ar matrix.[60] Under dilute propene conditions, an insertion product, H-V(η^3-allyl), was identified from the observed IR spectra. On the other hand, different isomers were proposed for metal ion reactions with propene.[29,32,33] For example, the Armentrout group investigated the reactions of propene with M^+ (M = Fe and Co) ions using guided-ion-beam spectrometry.[32,33] In their studies, a direct current discharge source was used to generate the M^+ ions, and a flow-tube reactor was used to produce thermalized $MC_3H_6^+$ formed by the condensation of M^+ and propene. These ions were then studied by threshold collisional activation, and the results were compared with the bimolecular reactivity of the M^+ ions. Their results indicated the possibility of both M^+(propene) and metallacyclobutane structures of $MC_3H_6^+$. Some evidence was also obtained for a third isomer, which was tentatively assigned to an inserted structure for $CoC_3H_6^+$.[33]

D. Formation of inserted and dehydrogenated species

Figure 7 presents the DFT computed stationary points for the formation of La(CHCCH$_3$), H—La(η^3-C$_3$H$_5$), and La(CHCHCH$_2$). These stationary points include reactants, intermediates (IMn), transition states (TSn), and products on the doublet potential energy surfaces. Relative energies are reported in Table S3. In the following discussion, we will focus on the concerted H_2 elimination for the formation of La(CHCCH$_3$) and La(CHCHCH$_2$) because previous studies have shown that step-wise dehydrogenation paths are less favorable for metal atom-mediated dehydrogenation.[40–42,44,47,61]

1. Formation of La(CHCCH$_3$)

La(CHCCH$_3$) is formed by 1,2-vinylic dehydrogenation. The first step is the exothermic formation of a π complex (IM1). The interaction between La and the vinylic carbons involves the donation of the propene π electrons to an empty La dσ orbital and the back donation from a La dπ orbital to a propene π* orbital. The resultant π complex is a metallacyclopropane with two La—C bonds and a C—C single bond. The breakage of the C=C π bond of propene is demonstrated by the elongation of the C—C bond from 1.331 to 1.504 Å and by the H atom bending off the LaCC plane. Similar three-membered metallacycles have also been identified by our group for La and Ce reactions with ethylene, acetylene, or propyne.[44–47] The second step of the reaction is the insertion of the La atom into C—H bonds. There are two types of C—H bonds in propene: vinylic and allylic C—H bonds. To form La(CHCCH$_3$), La first inserts into the vinylic C2 (middle C)—H bond of the propene molecule to yield inserted intermediate IM2. The insertion occurs through the transition state TS1, which is characterized by an imaginary C2—H stretching mode (834*i* cm^{-1}). From IM1 to IM2, the La—C1 bond is cleaved, a new La—H bond is formed, and the C1—C2 bond becomes a double bond (1.339 Å) again as in the free propene molecule. From IM2, the reaction proceeds with a La—H rotation via TS2 to yield a new intermediate (IM3). TS2 is characterized by an imaginary La—H rocking mode (140*i* cm^{-1}), and IM3 has a similar structure to IM2, except for the La—H bond reorientation. Because the La—H rotation costs very little energy, TS2 has nearly the same energies as IM2 or IM3. From IM3, a second insertion occurs between La and a vinylic C1(terminal C)—H bond of propene to form IM4. The transition state (TS3) between IM3 and IM4 is characterized by an imaginary C1—H stretching mode (879*i* cm^{-1}). The energy barrier of the second C—H insertion (TS3) is comparable to that of the first insertion (TS1). The similar energies of the two transition states may not be surprising as both C—H bonds are vinylic. The final step is the concerted H_2 elimination from IM4 to La(CHCCH$_3$) + H_2. No transition state was located between IM4 and the products. Because H_2 is very weakly bound to La in IM4, the dehydrogenation from H_2La(CHCCH$_3$) has a very small effect on the structure of the La(CHCCH$_3$) fragment. The whole 1,2-vinylic dehydrogenation process is predicted to be barrierless and exothermic by 14.9 kcal mol^{-1}.

2. Formation of H—La(η^3-C$_3$H$_5$) and La(CHCHCH$_2$)

The formation of both H—La(η^3-C$_3$H$_5$) and La(CHCHCH$_2$) begins with the formation of lanthanacyclopropane (IM1) as in the case of La(CHCCH$_3$) (Figure 7). However, instead of a vinylic C—H bond insertion, H—La(η^3-C$_3$H$_5$) (IM6) is formed by La inserting into an allylic C3—H bond in the methyl group. Because an allylic C—H bond (94.6 kcal mol^{-1}) is weaker than a vinylic C—H bond (111.1 kcal mol^{-1}), the insertion barrier from IM1 to TS4 is much lower (7.1 kcal mol^{-1}) than to TS1 (21.0 kcal mol^{-1}). The resultant intermediate IM5 undergoes a La—H rotation via TS5

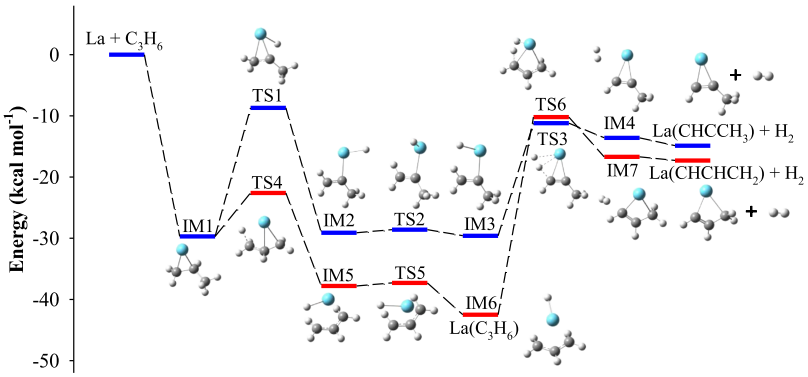

FIG. 7. Reaction pathways and energy profiles for the formation of La(CHCCH$_3$) via 1,2-dehydrogenation (blue trace), H—La(η^3-C$_3$H$_5$) via La insertion into an allylic C—H bond (red trace), and La(CHCHCH2) via 3,3-dehydrogenation (red trace) from the La + propene reaction at the DFT/B3LYP level, where IMn stands for intermediates and TSn for transition states.

to form IM6. IM5, TS5, and IM6 are all lower in energy than the corresponding stationary points IM2, TS2, and IM3 along the reaction coordinates of La(CHCCH$_3$). IM6 is the inserted species H—La(η^3-C$_3$H$_5$) identified by our MATI spectroscopic measurements. From IM6, La inserts into to a second C3—H bond via TS6 to form H$_2$La(CHCHCH$_2$) (IM7). The second insertion has a much higher energy barrier than the first one. The different energy barriers between the two insertion processes are due to the fact that the first insertion takes place in a weaker allylic C—H bond of the methyl group and the second occurs in a stronger vinylic C—H bond of the methylene group. The resulting H$_2$La(CHCHCH$_2$) intermediate then undergoes a concerted H$_2$ elimination to form La(CHCHCH$_2$). Again, because H$_2$ is weakly bound to the La atom in IM7, the dehydrogenation has practically no effect on the structure of La(CHCHCH$_2$). The whole process is exothermic by 17.3 kcal mol^{-1} and has no positive energy barrier. The La(CHCHCH$_2$) formation discussed above is through a 3,3-hydrogen elimination path. The metal-hydrocarbon radical could also be formed by 1,3-elimination (Figure S2). However, the computed 1,3-elimination pathway fails to involve the observed H—La(η^3-C$_3$H$_5$) species. This process is thus less likely.

IV. CONCLUSIONS

We have reported the MATI spectroscopic characterization of three La-hydrocarbon radicals formed by the C—H bond activation of propene. They are identified as H—La(η^3-C$_3$H$_5$), La(CHCCH$_3$), and La(CHCHCH$_2$). The C$_3$H$_5$ fragment in H—La(η^3-C$_3$H$_5$) is an allyl radical, La(CHCCH$_3$) is methyl-substituted metallacyclopropene, and La(CHCHCH$_2$) is metallacyclobutene. All three La-hydrocarbons species are in doublet ground states with a La-valence electron configuration of 6s^1, and the corresponding singly charged positive ions are in singlet states formed by the removal of the La 6s^1 electron. The adiabatic ionization energies of the three metal-hydrocarbon radicals are lower than that of the free metal atom as a result of the increased charge interaction in the ionic complexes. Metal-carbon or -hydrogen stretching and hydrocarbon-based bending frequencies are measured for these species. La(CHCCH$_3$) is formed by the concerted 1,2-vinylic H$_2$ elimination, whereas La(CHCHCH$_2$) by both allylic and vinylic dehydrogenation with H—La(η^3-allyl) being a reaction intermediate. In the future, we will attempt to investigate the structures of metal-hydrocarbon radicals formed by C—C bond breakage and coupling of propene.

SUPPLEMENTARY MATERIAL

See supplementary material for the geometries of La(CHCCH$_3$), La(CHCHCH$_2$), and H—La(η^3-C$_3$H$_5$) and their ion states; electronic states and energies of the three isomers of La(C$_3$H$_6$), energies of the stationary points along the reaction coordinates for the formation of three La-hydrocarbon radicals, and MATI spectra of La(C$_3$H$_6$) and simulations of its various isomers.

ACKNOWLEDGMENTS

We are grateful for the financial support from the National Science Foundation Division of Chemistry (Chemical Structure, Dynamics, and Mechanisms, Grant No. CHE-1362102). We also acknowledge additional support from the Kentucky Science and Engineering Foundation. S.K. thanks Tao Hong Li for the help in reaction pathway calculations.

[1] J. A. Labinger and J. E. Bercaw, Nature **417**, 507 (2002).
[2] R. G. Bergman, Nature **446**, 391 (2007).
[3] R. H. Crabtree, Chem. Rev. **110**, 575 (2010).
[4] T. B. Marder, P. W. Dyer, I. J. S. Fairlamb, S. Gibson, and P. Scott, Dalton Trans. **39**, 10321 (2010).
[5] J. Wencel-Delord, T. Droge, F. Liu, and F. Glorius, Chem. Soc. Rev. **40**, 4740 (2011).
[6] M. P. Doyle and K. I. Goldberg, Acc. Chem. Res. **45**(6), 777 (2012).
[7] P. L. Arnold, M. W. McMullon, J. Rieb, and F. E. Kuhn, Angew. Chem., Int. Ed. **54**, 82 (2015).
[8] K. Eller and H. Schwarz, Chem. Rev. **91**, 1121 (1991).
[9] J. C. Weisshaar, Acc. Chem. Res. **26**, 213 (1993).
[10] *Organometallic Ion Chemistry*, edited by B. S. Freiser (Kluwer, Dordrecht, 1996).
[11] D. K. Bohme and H. Schwarz, Angew. Chem., Int. Ed. **44**, 2336 (2005).
[12] J. Roithova and D. Schroeder, Chem. Rev. **110**, 1170 (2010).
[13] P. B. Armentrout, Catal. Sci. Technol. **4**, 2741 (2015).
[14] P. B. Armentrout, Int. J. Mass Spectrom. **377**, 54 (2015).
[15] M. T. Rodgers and P. B. Armentrout, Chem. Rev. **116**, 5642 (2016).
[16] B. Qiao, A. Wang, X. Yang, L. F. Allard, Z. Jiang, Y. Cui, J. Liu, J. Li, and T. Zhang, Nat. Chem. **3**, 634 (2011).
[17] G. Kyriakou, M. B. Boucher, A. D. Jewell, E. A. Lewis, T. J. Lawton, A. E. Baber, H. L. Tierney, M. Flytzani-Stephanopoulos, and E. C. Sykes, Science **335**, 1209 (2012).
[18] A. Figueroba, G. Kovacs, A. Bruix, and K. M. Neyman, Catal. Sci. Technol. **6**, 6806 (2016).
[19] J. Jones, H. Xiong, A. T. DeLaRiva, E. J. Peterson, H. Pham, S. R. Challa, G. Qi, S. Oh, M. H. Wiebenga, X. I. Pereira Hernandez, Y. Wang, and A. K. Datye, Science **353**, 150 (2016).
[20] W. Liu, L. X. Zhang, W. Yan, X. Liu, X. Yang, S. Miao, W. Wang, A. Wang, and T. Zhang, Chem. Sci. **7**, 5758 (2016).
[21] A. D. Brathwaite, T. B. Ward, R. S. Walters, and M. A. Duncan, J. Phys. Chem. A **119**, 5658 (2015).
[22] R. S. Walters, E. D. Pillai, P. V. R. Schleyer, and M. A. Duncan, J. Am. Chem. Soc. **127**, 17030 (2005).
[23] R. S. Walters, P. V. Schleyer, C. Corminboeuf, and M. A. Duncan, J. Am. Chem. Soc. **127**, 1100 (2005).
[24] S. R. Miller, T. P. Marcy, E. L. Millam, and D. G. Leopold, J. Am. Chem. Soc. **129**, 3482 (2007).
[25] R. B. Metz, Adv. Chem. Phys. **138**, 331 (2008).
[26] D. J. Brugh and M. D. Morse, J. Chem. Phys. **141**, 064304 (2014).
[27] M. A. Flory, A. J. Apponi, L. N. Zack, and L. M. Ziurys, J. Am. Chem. Soc. **132**, 17186 (2010).
[28] V. J. F. Lapoutre, B. Redlich, A. F. G. van der Meer, J. Oomens, J. M. Bakker, A. Sweeney, A. Mookherjee, and P. B. Armentrout, J. Phys. Chem. A **117**, 4115 (2013).
[29] C. Heinemann, D. Schroeder, and H. Schwarz, Chem. Ber. **127**, 1807 (1994).
[30] H. H. Cornehl, C. Heinemann, D. Schroeder, and H. Schwarz, Organometallics **14**, 992 (1995).
[31] J. Marcalo, M. Santos, A. P. de Matos, J. K. Gibson, and R. G. Haire, J. Phys. Chem. A **112**, 12647 (2008).
[32] R. H. Schultz and P. B. Armentrout, Organometallics **11**, 828 (1992).
[33] C. L. Haynes and P. B. Armentrout, Organometallics **13**, 3480 (1994).
[34] P. Mourgues, A. Ferhati, T. B. McMahon, and G. Ohanessian, Organometallics **16**, 210 (1997).
[35] V. Baranov, H. Becker, and D. K. Bohme, J. Phys. Chem. A **101**, 5137 (1997).
[36] P. B. Armentrout and Y. M. Chen, J. Am. Soc. Mass Spectrom. **10**, 821 (1999).
[37] D. Ritter, J. J. Carroll, and J. C. Weisshaar, J. Phys. Chem. **96**, 10636 (1992).
[38] J. J. Carroll, K. L. Haug, and J. C. Weisshaar, J. Am. Chem. Soc. **115**, 6962 (1993).
[39] J. J. Carroll, K. L. Haug, J. C. Weisshaar, M. R. A. Blomberg, P. E. M. Siegbahn, and M. Svensson, J. Phys. Chem. **99**, 13955 (1995).

[40]Y. Wen, M. Porembski, T. A. Ferrett, and J. C. Weisshaar, J. Phys. Chem. A **102**, 8362 (1998).
[41]M. Porembski and J. C. Weisshaar, J. Phys. Chem. A **105**, 6655 (2001).
[42]R. Z. Hinrichs, J. J. Schroden, and H. F. Davis, J. Phys. Chem. A **107**, 9284 (2003).
[43]J. J. Schroden and H. F. Davis, in *Modern Trend in Chemical Dynamics. II: Experiment and Theory*, Advanced Series in Physical Chemistry, Vol. 14, edited by X. Yang and K. Lium (World Scientific, Singapore, 2004), p. 215.
[44]S. Kumari, W. Cao, Y. Zhang, M. Roudjane, and D.-S. Yang, J. Phys. Chem. A **120**, 4482 (2016).
[45]Y. Zhang, M. W. Schmidt, S. Kumari, M. S. Gordon, and D.-S. Yang, J. Phys. Chem. A **120**, 6963 (2016).
[46]D. Hewage, W. R. Silva, W. Cao, and D.-S. Yang, J. Am. Chem. Soc. **138**, 2468 (2016).
[47]D. Hewage, M. Roudjane, W. R. Silva, S. Kumari, and D.-S. Yang, J. Phys. Chem. A **119**, 2857 (2015).
[48]B. R. Sohnlein, S. G. Li, J. F. Fuller, and D.-S. Yang, J. Chem. Phys. **123**, 014318 (2005).
[49]C. E. Moore, *Atomic Energy Levels* (National Bureau of Standards, Washington, DC, 1971).
[50]M. A. Duncan, T. G. Dietz, and R. E. Smalley, J. Chem. Phys. **75**, 2118 (1981).
[51]M. J. Frish, G. W. Trucks, H. B. Schlegel, G. E. Scuseria, M. A. Robb, J. R. Cheeseman, G. Scalmani, V. Barone, B. Mennucci, G. A. Petersson, H. Nakatsuji, M. Caricato, X. Li, H. P. Hratchian, A. F. Izmaylov, J. Bloino, and G. Zheng, GAUSSIAN 09, Revision A.01, Gaussian, Inc., Wallingford, CT, 2009.
[52]D.-S. Yang, J. Phys. Chem. Lett. **2**, 25 (2011).
[53]S. Li, "Threshold photoionization and ZEKE photoelectron spectroscopy of metal complexes," Ph.D. thesis, University of Kentucky, 2004.
[54]E. V. Doktorov, I. A. Malkin, and V. I. Man'ko, J. Mol. Spectrosc. **64**, 302 (1977).
[55]F. Duschinsky, Acta Physicochim. **7**, 551 (1937).
[56]D. R. Lide, *CRC Handbook of Chemistry and Physics*, 88th ed. (CRC, Boca Raton, FL, 2008).
[57]K. Schofield, J. Phys. Chem. A **110**, 6938 (2006).
[58]T. K. Todorova, I. Infante, L. Gagliardi, and J. M. Dyke, J. Phys. Chem. A **112**, 7825 (2008).
[59]J. F. Fuller, S. G. Li, B. R. Sohnlein, G. K. Rothschopf, and D.-S. Yang, Chem. Phys. Lett. **366**, 141 (2002).
[60]M. G. K. Thompson, S. W. C. Walker, and J. M. Parnis, Inorg. Chem. **50**, 7317 (2011).
[61]T. H. Li and X. G. Xie, J. Phys. Org. Chem. **23**, 768 (2010).

Mass-analyzed threshold ionization spectroscopy of lanthanum-hydrocarbon radicals formed by C—H bond activation of propene

Sudesh Kumari, Wenjin Cao, Dilrukshi Hewage, Ruchira Silva, and Dong-Sheng Yang

Citation: The Journal of Chemical Physics **146**, 074305 (2017); doi: 10.1063/1.4976316
View online: https://doi.org/10.1063/1.4976316
View Table of Contents: http://aip.scitation.org/toc/jcp/146/7
Published by the American Institute of Physics